

Next-to-leading order predictions for $WW + \text{jet}$ distributions at the LHC

John M. Campbell,

*Department of Physics and Astronomy,
University of Glasgow, Glasgow G12 8QQ, UK
Email: j.campbell@physics.gla.ac.uk*

R. Keith Ellis,

*Fermilab, Batavia, IL 60510, USA
Email: ellis@fnal.gov*

Giulia Zanderighi

*The Rudolf Peierls Centre for Theoretical Physics
Department of Physics, University of Oxford
1 Keble Road, OX1 3NP, Oxford, UK
Email: g.zanderighi1@physics.ox.ac.uk*

ABSTRACT: We present numerical results for the production of a W^+W^- pair in association with a jet at the LHC in QCD at next-to-leading order (NLO). We include effects of the decay of the massive vector bosons into leptons with spin correlations and contributions from the third generation of massive quarks. The calculation is performed using a semi-numerical method for the virtual corrections, and is implemented in MCFM. In addition to its importance *per se* as a test of the Standard Model, this process is an important background to searches for the Higgs boson and to many new physics searches. As an example, we study the impact of NLO corrections to $W^+W^- + \text{jet}$ production on the search for a Higgs boson at the LHC.

KEYWORDS: Higgs, QCD, Jets.

Contents

1. Introduction	1
2. Structure of the calculation	3
2.1 Lowest order	3
2.2 Real corrections	5
2.3 Virtual corrections	6
3. Results	7
3.1 Inclusive cuts	8
3.2 Application to the Higgs search	9
4. Conclusions	14
A. Triangle-Z production diagrams	15
B. Explicit numerical results	18

1. Introduction

The search for the Higgs boson at the Large Hadron Collider (LHC) will rely on analysing many types of events related to its different production and decay modes [1, 2]. If a Standard Model (SM) Higgs boson mass lies in the range $155 < m_H < 185$ GeV, the production of a Higgs boson that decays to W pairs, $H \rightarrow W^+W^-$, is expected to be a significant channel. It could even be the discovery mode for the Higgs boson, particularly if the mass of the Higgs boson lies very close to the threshold for the production of W pairs, $M_H = 2M_W$. Note that the W -bosons can both be real ($M_H \geq 2M_W$) or virtual ($M_H < 2M_W$).

There are two main mechanisms for producing a Higgs boson that leads to such final states at the LHC. The Higgs boson can be produced as the result of gluon fusion, with the Higgs boson coupling to an intermediate heavy quark loop (Fig. 1(a)), with further QCD radiation leading to additional jets being observed in the final state. Alternatively, the Higgs boson may be produced with a sizeable cross section via weak boson fusion (WBF - see Fig. 1(b)), in which the decay products of the Higgs boson are naturally accompanied by two forward jets. Therefore the channel W^+W^- accompanied by 0, 1 or 2 jets will be subject to intense scrutiny at the LHC and all SM backgrounds should be investigated as fully as possible.

If such a Higgs boson exists, the $WW + 0$ jet sample is expected to contain events originating from a Higgs boson that is predominantly produced via gluon fusion, with the

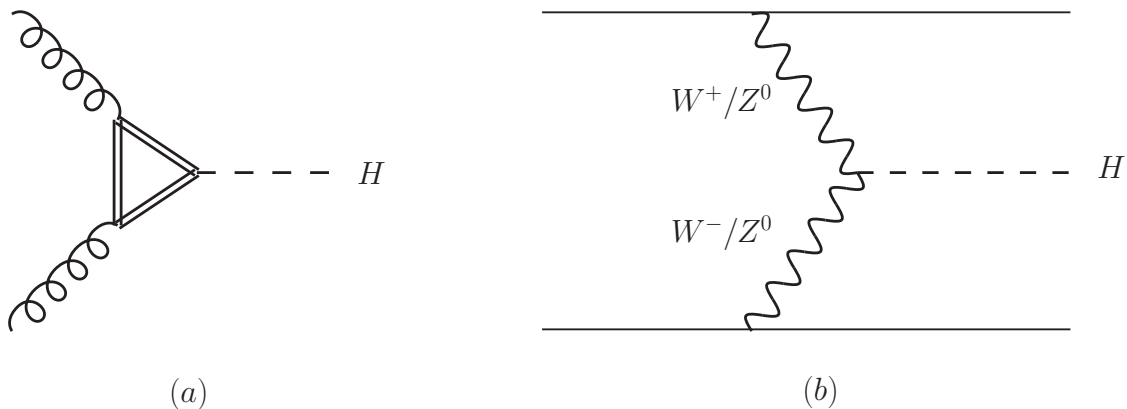


Figure 1: The two primary mechanisms for producing a Higgs boson in association with jets at the LHC.

largest background being the normal QCD production of WW pairs. This signal has been calculated not only to NLO [3, 4] but also up to NNLO [5, 6], whilst the NLO corrections to this background are also known [7, 8, 9].

If instead the sample is selected by requiring two forward jets then the putative Higgs boson is preferentially produced via the WBF mechanism. This is now expected to be the single most significant channel in the range $130 < m_H < 190$ GeV (see for example Ref. [10]). In this case, the signal has been known to NLO for some time [11, 12, 13], whilst the NLO calculation of the dominant background from the production of $WW + 2$ jets is currently unknown.

It has recently been suggested that the Higgs signal significance can be improved by considering also the final state which consists of the leptonic decays of W -pairs, plus at least one additional jet [14]. In this study, only a single jet is demanded at large rapidity. This has the effect of substantially reducing the backgrounds whilst not unduly compromising the signal because of the nature of the WBF events. This renders such a search feasible, albeit with significant SM backgrounds whose size should clearly be assessed beyond the LO approximation. Dominant among these is the production of $WW + \text{jet}$, the NLO corrections to which we present in this paper. Since the final state is identified through the leptonic decay modes of the W^+W^- system to $\ell^+\ell^-$ and missing energy, we include in our calculation the leptonic decays of the W 's and their spin correlations¹. The calculation is performed using a recently-developed semi-numerical method for computing virtual 1-loop corrections [16, 17, 18].

The importance of this calculation has already been recognized by its appearance on the list of next-to-leading order priorities assembled at the Les Houches workshop in

¹In the final stages of preparation of this paper, an independent calculation of this process has been presented [15]. The results of that calculation appear consistent with the ones indicated by this paper, although Ref. [15] does not contain an evaluation of the NLO corrections at a specific phase space point that we could exactly compare with in a straightforward way. We note however that the calculation of Ref. [15] does not include the decay products of the W bosons and their correlations.

2005 [19]. This is motivated largely by its obvious importance to the search for the Higgs boson and for other signals of new physics at the LHC. Nevertheless, the WW +jet process is interesting in its own right as a test of our theoretical understanding of the SM. In the same way that the SM has been probed experimentally at the Tevatron by measurements of the WW and W + jets cross sections (for recent examples, see Refs. [20] and [21]), the rate of events at the LHC will allow similar studies of WW +jet events at even higher energy scales. In addition, this calculation is a necessary stepping stone to highly-desired NLO calculations of $2 \rightarrow 4$ processes such as the aforementioned $WW + 2$ jet process [19], as well as $W + 3$ jet production.

The structure of the paper is as follows. In section 2 we discuss the overall structure of the calculation, with attention paid to the finite contribution arising from internal loops of massive quarks. Section 3 presents the results of our calculation with two types of event selection, one indicative of a typical inclusive analysis at the LHC and the other relevant for a search for the Higgs boson. To that end, we perform a parton-level analysis of all the major background processes using the general purpose NLO program MCFM [8]. Our conclusions are contained in section 4. Finally, the appendices consist of analytical results for some of the massive triangle diagrams that appear in our calculation, together with explicit numerical results for the 1-loop corrections at a particular phase space point.

2. Structure of the calculation

2.1 Lowest order

Let us consider as the lowest order, $\mathcal{O}(\alpha_{\text{ew}}^4 \alpha_s)$, reference process the one in which the up quarks annihilate into a W^+W^- pair,

$$0 \rightarrow u(p_1) + \bar{u}(p_2) + W^+(\ell(p_3) + \bar{\ell}(p_4)) + W^-(\ell(p_5) + \bar{\ell}(p_6)) + g(p_7). \quad (2.1)$$

The Feynman diagrams and the momentum assignments are shown in Fig. 2. All momenta are outgoing. The results for a positive helicity gluon and left handed quark line are determined in terms of the two primitive amplitudes given below [22]²,

$$A_7^{(a)} = \frac{\langle 15 \rangle}{\langle 17 \rangle s_{56} s_{34} s_{156}} \left[\frac{\langle 15 \rangle [56] [42] \langle 3|2 + 4|7 \rangle}{s_{234}} + \frac{\langle 3|1 + 5|6 \rangle \langle 1|2 + 7|4 \rangle}{\langle 27 \rangle} \right], \quad (2.2)$$

$$A_7^{(b)} = \frac{1}{\langle 17 \rangle \langle 27 \rangle s_{56} s_{34} s_{127}} \left[\langle 15 \rangle \langle 1|2 + 7|6 \rangle \langle 3|5 + 6|4 \rangle \right. \\ \left. - \langle 13 \rangle \langle 1|2 + 7|4 \rangle \langle 5|3 + 4|6 \rangle - \langle 35 \rangle [46] \langle 1|(3 + 4)(2 + 7)|1 \rangle \right], \quad (2.3)$$

where $s_{ij} = (p_i + p_j)^2$, $s_{ijk} = (p_i + p_j + p_k)^2$. $\langle ij \rangle$ and $[ij]$ are the standard spinor products for massless vectors such that $\langle ij \rangle [ji] = s_{ij}$. The results for other helicities may be obtained

²Note that apart from the overall sign, this agrees with the result obtained in [22] Eqs.(2.22) and (2.23) for $0 \rightarrow u(p_1) + \bar{u}(p_2) + W^-(\ell(p_3) + \ell(p_4)) + W^+(\ell(p_5) + \ell(p_6)) + g(p_7)$.

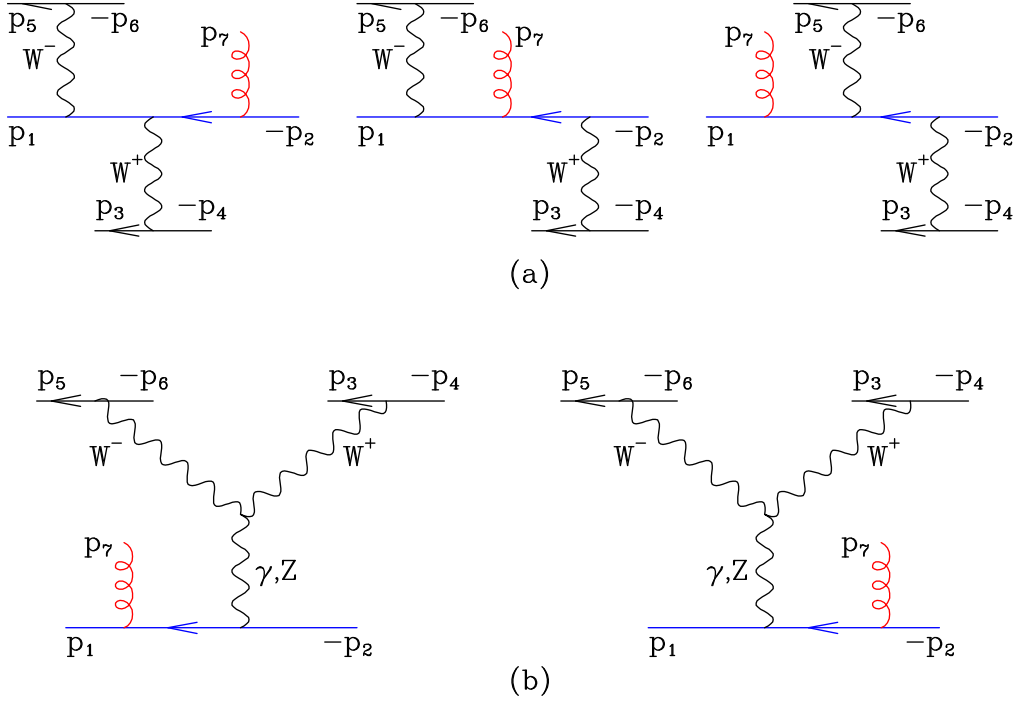


Figure 2: Leading order diagrams for up quark annihilation to $W^+W^- + g$.

by permutations of the results in Eqs. (2.2, 2.3). Since we are interested in $W^+W^- + \text{jet}$ as a background to Higgs boson or new physics searches, we need to go beyond the zero-width approximation and in general we have $q_V^2 \neq M_V^2$. We introduce the W propagators with a Breit-Wigner form,

$$P_W(s) \equiv \frac{s}{s - M_W^2 + i\Gamma_W M_W}. \quad (2.4)$$

If needed one can also introduce a width for the Z -boson. To do this in a gauge invariant (though not unique) way one can multiply the whole amplitude by an additional factor [23, 24],

$$P_Z(s) \equiv \frac{s - M_Z^2}{s - M_Z^2 + i\Gamma_Z M_Z}. \quad (2.5)$$

To obtain the full amplitude the results of Eqs.(2.2, 2.3) must be dressed with appropriate couplings,

$$\begin{aligned} \mathcal{A}^A(u_1^L, \bar{u}_2^R, \nu_3, e_4^+, \mu_5^-, \bar{\nu}_6, g_7^R) = \\ \sqrt{2} t_{i_1 i_2}^A H \left[A_7^{(a)}(1, 2, 3, 4, 5, 6, 7) + C_{L, \{u\}}(s_{127}) A_7^{(b)}(1, 2, 3, 4, 5, 6, 7) \right], \\ \mathcal{A}^A(u_1^R, \bar{u}_2^L, \nu_3, e_4^+, \mu_5^-, \bar{\nu}_6, g_7^R) = \sqrt{2} t_{i_1 i_2}^A H \left[C_{R, \{u\}}(s_{127}) A_7^{(b)}(2, 1, 3, 4, 5, 6, 7) \right], \end{aligned} \quad (2.6)$$

where the couplings $C_{L, \{u\}}$ and $C_{R, \{u\}}$ that appear will be defined shortly and H is an

overall factor given by,

$$H = ig_s g_W^4 P_W(s_{34}) P_W(s_{56}) P_Z(s_{127}). \quad (2.7)$$

The corresponding results for processes involving d quarks can be written as follows,

$$\begin{aligned} \mathcal{A}^A(d_1^L, \bar{d}_2^R, \nu_3, e_4^+, \mu_5^-, \bar{\nu}_6, g_7^R) = \\ \sqrt{2} t_{i_1 i_2}^A H \left[A_7^{(a)}(1, 2, 5, 6, 3, 4, 7) + C_{L, \{d\}}(s_{127}) A_7^{(b)}(1, 2, 5, 6, 3, 4, 7) \right], \\ \mathcal{A}_d^A(d_1^R, \bar{d}_2^L, \nu_3, e_4^+, \mu_5^-, \bar{\nu}_6, g_7^R) = \sqrt{2} t_{i_1 i_2}^A H \left[C_{R, \{d\}}(s_{127}) A_7^{(b)}(2, 1, 5, 6, 3, 4, 7) \right], \end{aligned} \quad (2.8)$$

where we now specify the left- and right-handed couplings of up- and down-type quarks as,

$$C_{L, \{u\}}(s) = \pm \left[2Q \sin^2 \theta_W + \frac{s(2T_3^f - 2Q \sin^2 \theta_W)}{s - M_Z^2} \right], \quad (2.9)$$

$$C_{R, \{u\}}(s) = \pm 2Q \sin^2 \theta_W \left[1 - \frac{s}{s - M_Z^2} \right]. \quad (2.10)$$

In these formulae, $T_3^f = \pm \frac{1}{2}$ and t_{ij}^A is the colour matrix in the fundamental representation for the emitted gluon, normalized so that $\text{Tr}(t^A t^B) = \frac{1}{2} \delta^{AB}$. g_s represents the strong coupling and the weak coupling is related to the Fermi constant by $g_W^2 / (8M_W^2) = G_F / \sqrt{2}$. The extra sign for the d -type quarks is due to the fact that the triple boson term does not require the shift ($3 \leftrightarrow 5, 4 \leftrightarrow 6$) when we go from u to d . If it is included anyway then an extra minus sign results.

The leading order cross-section is obtained by considering all possible crossings of the quarks and gluon and by summing the squared amplitudes for all final state helicities and averaging over the spin and colour of the initial state partons. At leading order the cross-section receives contributions from processes with an incoming quark-antiquark pair or with one (anti-)quark and one gluon in the initial state.

2.2 Real corrections

The real matrix element corrections to $W^+W^- + 1$ jet production are obtained by including all crossings of results for the two basic processes,

$$\begin{aligned} 0 &\rightarrow u(p_1) + \bar{u}(p_2) + W^+(\ell(p_3) + \bar{\ell}(p_4)) + W^-(\ell(p_5) + \bar{\ell}(p_6)) + g(p_7) + g(p_8), \\ 0 &\rightarrow u(p_1) + \bar{u}(p_2) + W^+(\ell(p_3) + \bar{\ell}(p_4)) + W^-(\ell(p_5) + \bar{\ell}(p_6)) + q'(p_7) + \bar{q}'(p_8). \end{aligned} \quad (2.11)$$

These tree-level matrix elements have been checked against the results of Madgraph [25]. At $\mathcal{O}(\alpha_{\text{ew}}^4 \alpha_s^2)$ the cross-section receives contributions from processes with two incoming gluons and a qq ($\bar{q}\bar{q}$)-pair as well. Soft and collinear singularities are handled using the dipole subtraction scheme [26].

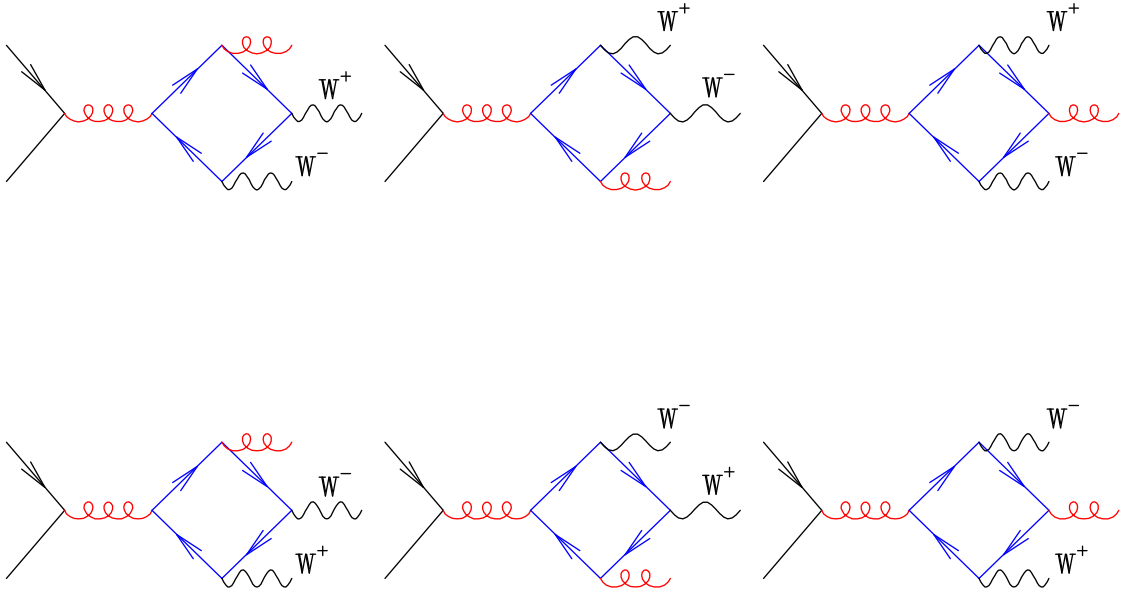


Figure 3: Fermion loop diagrams with W^+W^- contributing at one loop.

2.3 Virtual corrections

For the virtual corrections we have to consider one-loop QCD corrections to the tree-level processes in figure 2. We have altogether 30 diagrams where the W -bosons are attached directly to the incoming quark lines and which result from dressing the diagrams of figure 2(a) with virtual gluons. In addition, we have the 6 diagrams of Fig. 3 which have two charged bosons attached to a fermion loop.

There are 11 diagrams which result from dressing the diagrams of Fig. 2b with virtual gluons. In addition there are the four diagrams of Fig. 4 which have a Z boson attached to a fermion loop and 6 bubble diagrams with a fermion loop which vanish trivially because of colour conservation. The full one-loop virtual corrections we consider here involve fermionic corrections coming from two massless families circulating in the closed fermion loop and from a third massive generation, $m_b \neq m_t \neq 0$. (We could as well choose to set $m_b \rightarrow 0$ and keep only m_t finite).

The massless contribution to the virtual matrix elements have been computed using the semi-numerical approach presented in Refs. [16, 17, 18] based on Davydychev reduction of tensor integrals followed by scalar reduction of higher dimensional scalar integrals. Results were checked using a second method based on Passarino-Veltman reduction [27]. The method is considerably more efficient than the one used for [28, 29, 30] since we have now a booking of computed integrals not only for higher dimensional scalar integrals, but also for tensor ones.

An additional complication compared to the applications of the semi-numerical method considered before is that we have closed fermion traces involving one or two γ_5 matrices. We adopt the t'Hooft-Veltman prescription and split γ_μ matrices into a four-dimensional part $\hat{\gamma}_\mu$ which anti-commutes with γ_5 and an ϵ -dimensional part $\tilde{\gamma}_\mu$ which commutes with

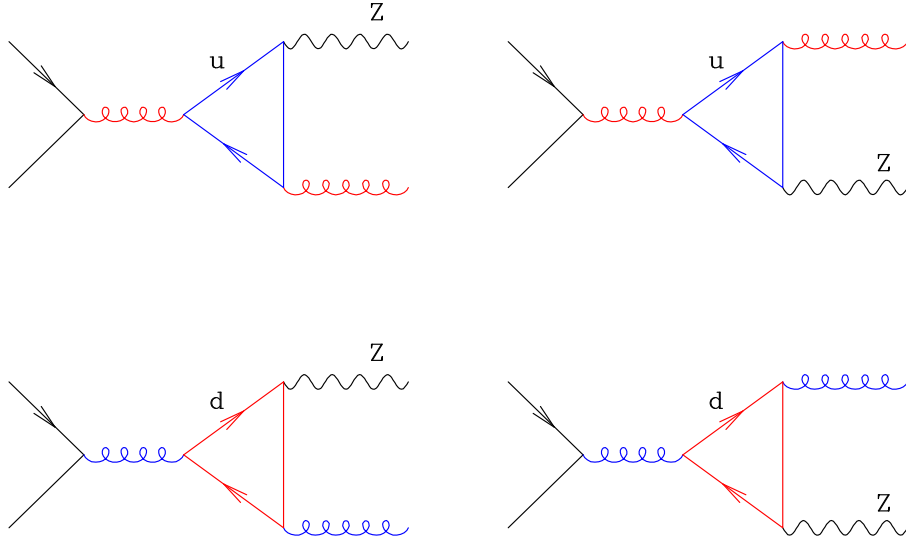


Figure 4: Fermion loop diagrams with Z contributing at one loop.

γ_5 ,

$$\gamma_\mu = \hat{\gamma}_\mu + \tilde{\gamma}_\mu, \quad \{\hat{\gamma}_\mu, \gamma_5\} = 0, \quad [\tilde{\gamma}_\mu, \gamma_5] = 0. \quad (2.12)$$

For the massive contributions we have to consider box diagrams with two W bosons attached to the loop, shown in Fig. 3 and triangle diagrams where a Z boson is attached to the quark loop shown in Fig. 4. We computed the triangle diagrams both fully analytically (results are given in App. A) and numerically using LoopTools [31]. Box integrals have been computed only numerically. Results for these amplitudes, as well as for the massless amplitudes, are given in Appendix B for one randomly chosen phase space point.

The whole calculation is incorporated into a private version of the general-purpose next-to-leading order code MCFM [8]. The code is flexible enough to allow running with on-shell or off-shell bosons.

3. Results

In the following we present for results for $W^+W^- + \text{jet}$ production at the LHC (pp collisions, $\sqrt{s} = 14$ TeV). We use the following electroweak parameters:

$$\begin{aligned} M_Z &= 91.188 \text{ GeV}, & M_W &= 80.419 \text{ GeV}, & M_H &= 170 \text{ GeV}, \\ \Gamma_Z &= 2.49 \text{ GeV}, & \Gamma_W &= 2.06 \text{ GeV}, & G_F &= 1.1663910^{-5}, \end{aligned}$$

and furthermore we have,

$$m_t = 172.5 \text{ GeV}, \quad \Gamma_t = 1.48 \text{ GeV}, \quad m_b = 4.62 \text{ GeV}. \quad (3.1)$$

For the calculation of $WW + \text{jet}$ at NLO (LO) we use MRST2004f4nlo (MRST2004f4lo) parton distribution functions corresponding to $\alpha_s(M_Z) = 0.1137$ ($\alpha_s(M_Z) = 0.1251$) [32]. Furthermore we use a four-flavour running and four-flavour evolution of pdfs and the sum

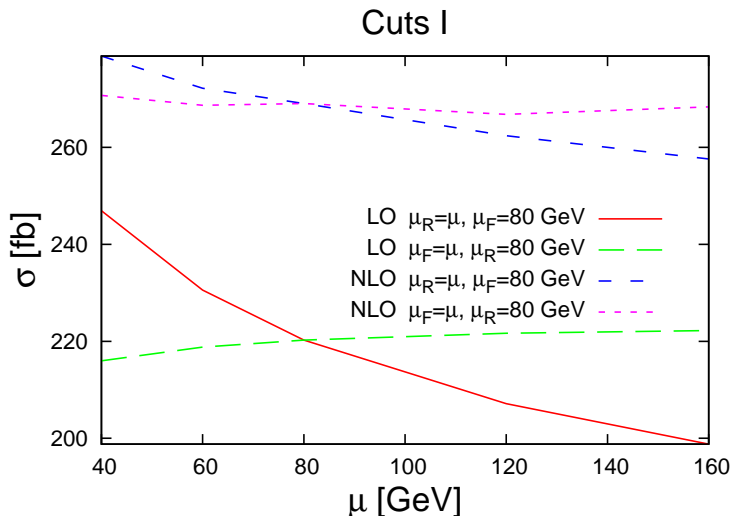


Figure 5: Scale dependence for the cross section with cuts I only, as specified in the text.

over partons in the incoming protons runs over light partons only (d, u, s, c). When we consider the Higgs search in section 3.2 we use standard, five-flavour parton densities with five-flavour running of the coupling for the signal processes and all backgrounds other than $WW+\text{jet}$. Specifically, we use MRST2004 [33]. To define a jet we run the inclusive k_T algorithm with $R = 0.6$. In the following we consider two sets of cuts, a more inclusive one and one designed to suppress QCD $W^+W^- + 1$ jet events and other backgrounds compared to $H(\rightarrow W^+W^-) + 1$ jet.

3.1 Inclusive cuts

We consider first a fairly minimal set of cuts to examine the effect of the NLO corrections to the $WW+\text{jet}$ process in an inclusive study. We require at least one jet with,

$$P_{t,j1} > 30 \text{ GeV}, \quad |\eta_{j1}| < 4.5, \quad (3.2)$$

and then some basic requirements on the decay products of the W 's: a minimum missing transverse energy and two opposite sign charged leptons with,

$$P_{t,\text{miss}} > 30 \text{ GeV}, \quad P_{t,\ell_1} > 20 \text{ GeV}, \quad P_{t,\ell_2} > 10 \text{ GeV}, \quad |\eta_{\ell_1(\ell_2)}| < 2.5. \quad (3.3)$$

Furthermore we require the leptons to be isolated, i.e. we impose,

$$R_{j,\ell_1} > 0.4, \quad R_{j,\ell_2} > 0.4, \quad R_{\ell_1,\ell_2} > 0.2. \quad (3.4)$$

Together, we refer to the cuts in equations (3.2), (3.3) and (3.4) collectively as ‘‘cuts I’’.

In figure 5 we plot the total cross section with cuts I. We fix the renormalization scale (or the factorization scale) to be equal to 80 GeV and vary the other scale around this value. We see that the NLO correction is sizeable, of the order of 25%, and that this is not covered by the scale variation of the LO prediction. While the factorization scale dependence is quite mild both at LO and at NLO, the dominant variation is due to the renormalization scale. This dependence is reduced by roughly a factor two at NLO.

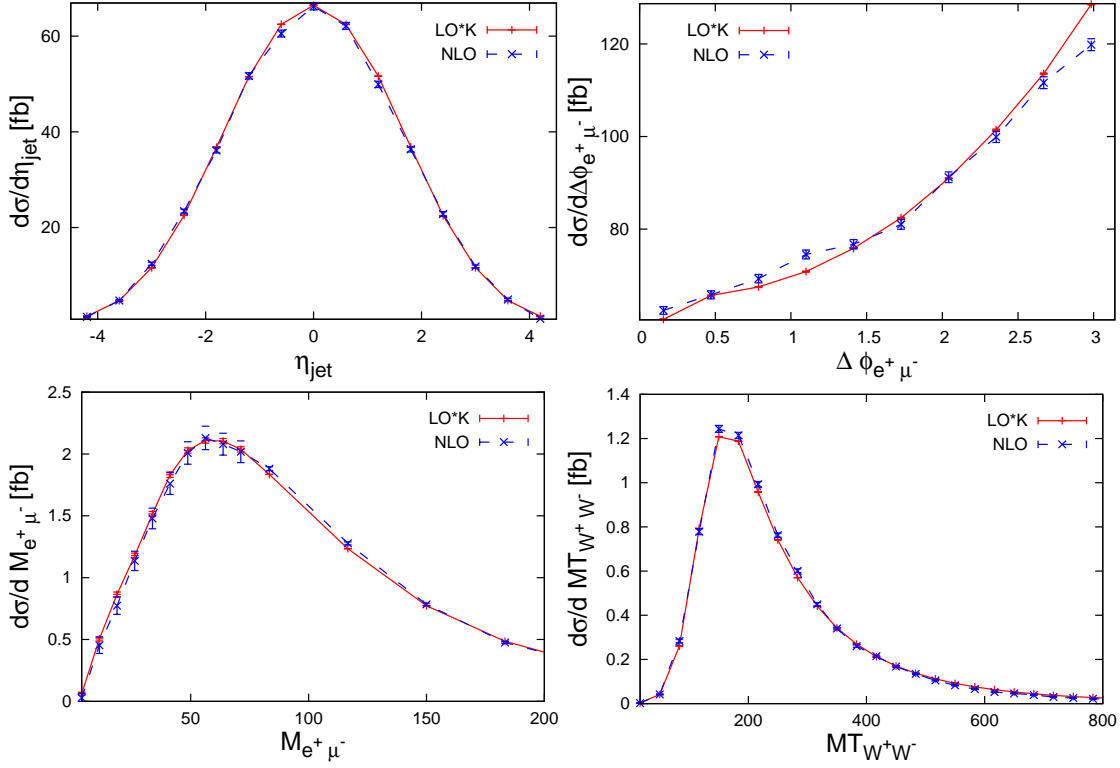


Figure 6: A comparison of the shapes of various kinematical distributions in the WW +jet process at LO and NLO with cuts I. The observable $M_{T,WW}$, the transverse mass of the W^+W^- pair, is defined by equations (3.5) and (3.6).

Since our calculation is implemented in the parton-level Monte Carlo program MCFM, we are also able to examine the effect of the QCD corrections on any infrared-safe observable. In Figure 6 we compare the LO and NLO predictions at $\mu_F = \mu_R = 80$ GeV for a few examples of distributions that are often important in experimental analyses: the rapidity η_{jet} of the leading jet, the azimuthal angle $\Delta\phi_{e\mu}$ between the two charged leptons, the invariant mass of the two charged lepton system $M_{e\mu}$ and the transverse mass of the W^+W^- pair defined as in Ref. [34],

$$M_{T,WW} = \sqrt{(\cancel{E}_T + E_{T,e\mu})^2 - (\cancel{\vec{p}}_T + \vec{p}_{T,e\mu})^2}, \quad (3.5)$$

where,

$$E_{T,e\mu} = \sqrt{\vec{p}_{T,e\mu}^2 + M_{e\mu}^2}, \quad \cancel{E}_T = \sqrt{\vec{p}_T^2 + M_{e\mu}^2}. \quad (3.6)$$

We have rescaled the LO prediction by the K -factor which can be read out of table 1 so as to be able to compare the shapes of the distributions. The results indicate that the shapes of the LO distributions are mostly unchanged at NLO.

3.2 Application to the Higgs search

As mentioned already, the WW +jet process is expected to be a significant background to the $H(\rightarrow WW)$ +jet search channel at the LHC. In this channel there are two mechanisms by which the Higgs boson can be produced:

for which the NLO corrections are known and sizeable [38]. In this study events in which two W 's and only one b -quark are observed are considered part of the NLO corrections to process (d). This background assumes that both b -quarks are observed and it contributes because our signal contains one or more jets. Although the corrections to the $t\bar{t}$ process are included in MCFM, this does not include the decay of the top quarks. Since we require cuts on the leptons produced in the top quark decays, we therefore limit our study of this process to LO only.

- (f) A process analogous to the one which we consider in this paper, Z -pair+jet production,

$$q + \bar{q} \rightarrow ZZ + g . \quad (3.12)$$

$$\left. \begin{array}{l} \downarrow \\ \downarrow \end{array} \right\} \begin{array}{l} \rightarrow \nu\bar{\nu} \\ \rightarrow e^+e^- \end{array}$$

The NLO corrections to this process are currently unknown and could be computed precisely as those for $q\bar{q} \rightarrow WW + g$ presented in this paper. Accordingly, MCFM implements currently only the LO contribution. We will see however, that the cross-section for this process is very small, so that no NLO corrections are required.

- (g) The production of W -pairs by EW processes, e.g.

$$u + d \rightarrow W^-W^+ + d + u . \quad (3.13)$$

This process is known at NLO [39], but is not implemented in MCFM. Given that its cross-section turns out to be very small, we have calculated only its leading order contribution by using the Madgraph package [25].

In order to suppress the backgrounds (c)–(g) with respect to the Higgs boson signal processes (a) and (b), we follow the strategy of Ref. [14] and apply cuts on four additional variables. The shapes of the distributions for both the signal and backgrounds are shown in Figure 7, with only the inclusive set of cuts (“cuts I”) applied. The signal processes are calculated using a putative Higgs mass of 170 GeV, above the threshold for production of two real W 's.

In these figures all the curves have been normalized to unit area to indicate only their shape, with the corresponding cross sections given in table 1. We notice that with cuts I the $t\bar{t}$ process is by far the dominant background. Furthermore, since process (g) has only a very small cross section even with this minimal set of cuts, we do not plot the corresponding distributions in Figure 7 and do not consider it in the analysis any further.

From these plots, it is clear that WBF production of the Higgs boson is associated with two jets forward in rapidity. Therefore, in addition to our previous selection (“cuts I”), we require that the leading jet and the second jet, if present, should be in the forward region,

$$|\eta_{j_1}| > 1.8 \quad |\eta_{j_2}| > 2.5 . \quad (3.14)$$

Furthermore, the azimuthal angle between the charged leptons and their invariant mass should satisfy,

$$\phi_{\ell_1, \ell_2} < 1.2 \quad m_{\ell_1, \ell_2} < 75 \text{ GeV} . \quad (3.15)$$

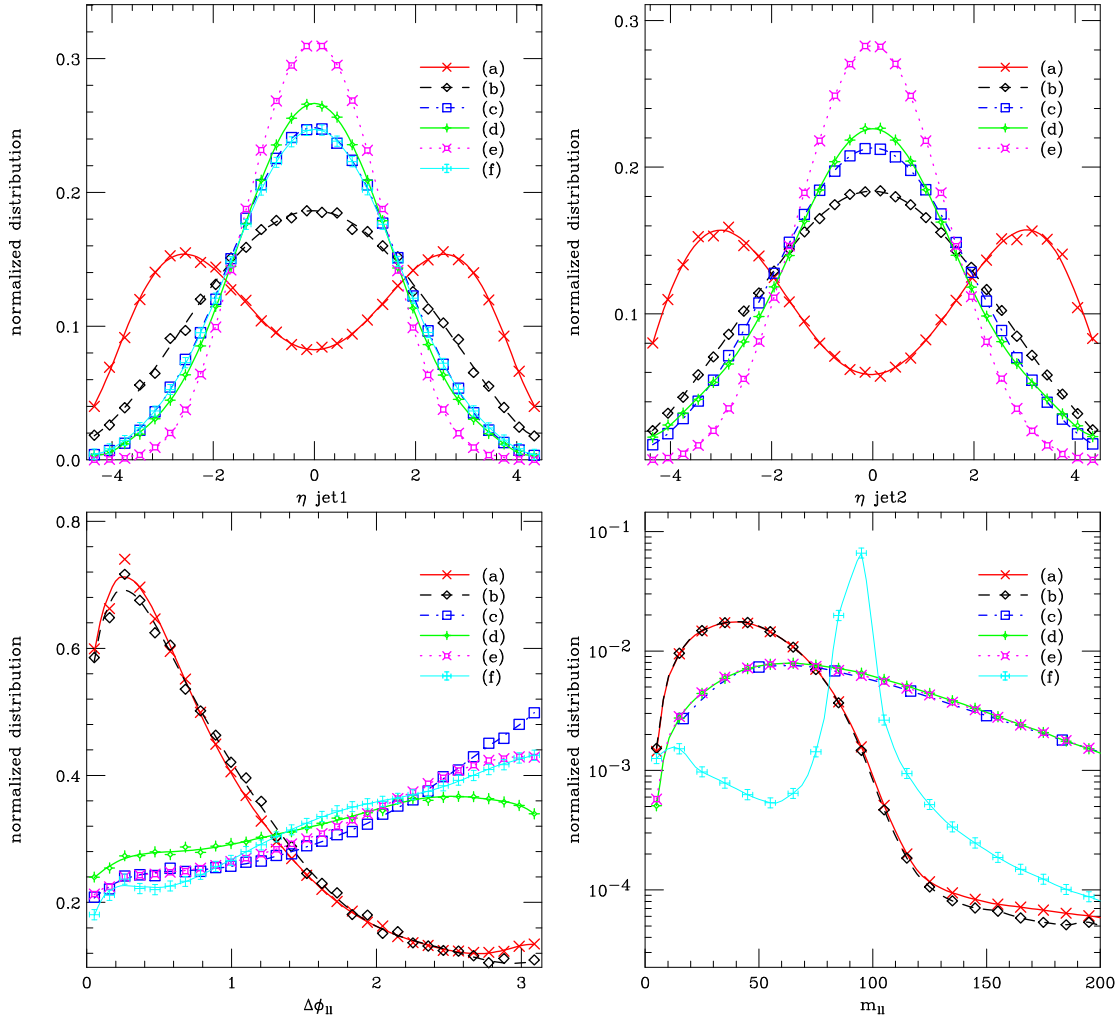


Figure 7: Shapes of the signal and background distributions for the rapidities of the leading and sub-leading jets (top-left and top-right respectively), the angle between the two leptons (bottom-left) and the invariant mass of the lepton pair (bottom-right). The curves shown are: (a) Higgs production by WBF (red); (b) by gluon fusion (black); (c) WW +jet (blue); (d) $W + t$ (green); (e) $t\bar{t}$ (magenta); and (f) ZZ +jet (cyan). The two Higgs production modes (by WBF and by gluon fusion) and single top production are calculated at NLO.

The first of these cuts is a clear discriminator between the two Higgs boson signals and all the backgrounds, whilst the second particularly discriminates against the background from ZZ +jet and top quark events. We refer to the cuts in equations (3.14) and (3.15) as “cuts II”.

In figure 8 we examine the scale dependence of the WW +jet background cross section with the additional cuts applied. There is a very large increase in the cross section going from LO to NLO and we see very little improvement in scale dependence. These very large corrections are typical of calculations in which new sub-processes enter at NLO. For WW +jet, the only contributions at LO are from $q\bar{q}$, qg and $\bar{q}g$ initial states. At NLO, in the real radiation term, one has also gg and qq ($q\bar{q}$) initial states. In particular, the qq -type

Table 1: Cross sections (fb) for signal and background cross sections, using cuts I only, as described in the text.

Process	σ_{LO} (fb)	σ_{NLO} (fb)
(a) $H \rightarrow WW$ (WBF)	22.5	22.3
(b) $H \rightarrow WW$ (gluon fusion)	35.9	64.5
(c) WW +jet	220	269
(d) $W + t$	210	216
(e) $t\bar{t}$	3090	-
(f) ZZ +jet	36.3	-
(g) WW +2 jets (EW)	9.3	-

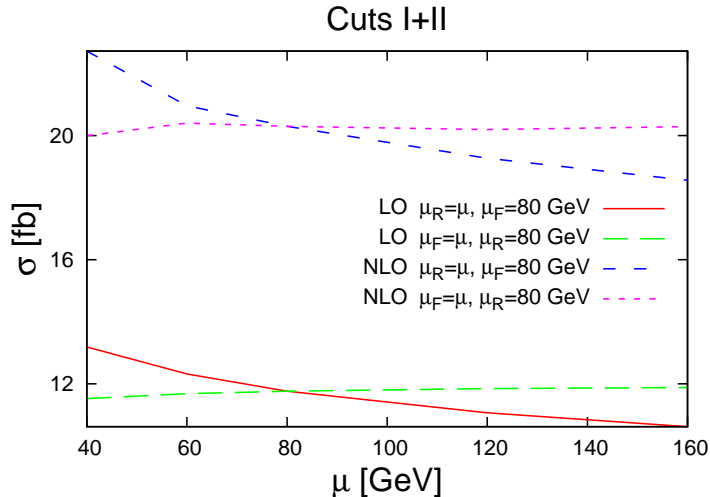


Figure 8: Scale dependence for the cross section with the cuts I and II.

processes are very similar kinematically to the WBF Higgs signal. Therefore when cuts II are applied, there is a large contribution from the qq initial state since the cuts cannot suppress such “signal-like” sub-processes.

The cross sections for the signal and background processes, after both cuts I and II have been applied, are collected in table 2. From the cross sections given in this table we see that the cuts have been effective in reducing the backgrounds compared to the signal processes. Comparing with table 1, we see that the WBF signal process is reduced by about a factor of 2 and the gluon fusion process by a factor of 3.5. In contrast, the huge backgrounds from top pair production and single top production have been reduced by factors of about 300 and 30 respectively. The ZZ +jet process has been rendered negligible as a background by the cut on the invariant mass of the lepton pairs. For the WW +jet process which we have calculated in this paper, the cuts reduce the cross section by a factor of 20 at LO. However, since the NLO correction amounts now to around 70%, the overall reduction of the QCD production of $WW + 1$ jet at NLO is only by a factor of about 14. As a result this process is the dominant source of background events in our

Table 2: Cross sections (fb) for signal and background cross sections, using cuts I+II, as described in the text.

Process	σ_{LO} (fb)	σ_{NLO} (fb)
(a) $H \rightarrow WW$ (WBF)	10.6	10.6
(b) $H \rightarrow WW$ (gluon fusion)	8.6	18.0
(c) WW +jet	11.7	20.2
(d) $W + t$	7.8	7.6
(e) $t\bar{t}$	12.7	-
(f) ZZ +jet	0.44	-

analysis, although a naive estimate of S/\sqrt{B} from this table is about 1. We note however that we have not included NLO effects in the estimate of the top pair background. For the totally inclusive top cross section, using our choice of parameters, the enhancement from LO to NLO corresponds to a K -factor of approximately 1.5. It is therefore reasonable to expect that the top pair cross section would also increase at NLO in the phase space region selected by cuts I and II. Therefore we expect the WW +jet and $t\bar{t}$ backgrounds to be comparable and a significant source of background events in this channel.

4. Conclusions

In this paper we have computed the NLO QCD corrections to the production of W pairs in association with a jet at hadron colliders, a calculation highly desired by the experimental community [19]. The calculation is performed using a semi-numerical approach and implemented in the general purpose NLO code MCFM. We find that, for cuts typical of LHC analyses, in which a jet is defined with transverse momentum above 30 GeV, the effect of the QCD corrections is to increase the cross section by 25% for our default scale choice ($\mu_F = \mu_R = 80$ GeV). Dependence on the renormalization and factorization scales at NLO is mild and is decreased by about a factor of two compared to LO.

We have also performed a parton level analysis of the impact of these QCD corrections on the search for a Higgs boson of mass 170 GeV at the LHC, using the channel $H \rightarrow W^+W^- + \text{jet}$. Including the effect of NLO corrections also in the signal processes, Higgs production by gluon fusion and by WBF, we find that the WW +jet background is one of the dominant backgrounds and is comparable to the WBF signal. In this analysis we have used a tighter set of cuts to select the WBF events and to suppress the large QCD backgrounds. We find that these cuts enhance the effect of the NLO corrections to WW +jet, which now increase the LO cross section by 70% in this region. We conclude that any studies of the Higgs boson search in this channel must take into account this significant correction to the number of expected background events.

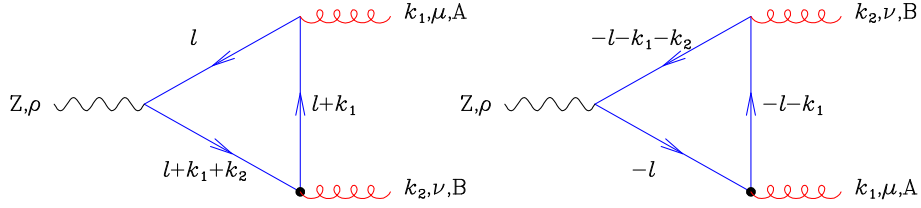


Figure 9: Triangle diagrams with closed fermion loops.

Acknowledgments

JC and GZ thank the Galileo Galilei Institute for Theoretical Physics for their hospitality and the INFN for partial support during the final stages of this work. GZ is grateful to Zuerich University for hospitality and the use of computer facilities. We also thank Babis Anastasiou, Michael Dittmar and Bill Quayle for discussions and we acknowledge correspondence and comparison of intermediate results with Gregory Sanguinetti and Stefan Karg.

A. Triangle-Z production diagrams

In this appendix we give analytical results for triangle diagrams where a Z is emitted from a closed fermion loop. Contributions where a Higgs is emitted are included in the signal process b), eq. 3.8. Results are valid for an arbitrary value of the mass m of the quarks in the loop.

We calculate the triangle shown in Fig. 9, where all momenta are outgoing $k_1 + k_2 + k_3 = 0$ and to begin with $k_1^2 \neq 0, k_2^2 \neq 0$. The result for the two triangle diagrams (including the minus sign for a fermion loop) is,

$$T_{AB}^{\mu\nu\rho}(k_1, k_2) = i \frac{g_s^2}{16\pi^2} \frac{1}{2} \delta_{AB} \left(\frac{g_W}{2 \cos \theta_W} \right) T_3^f \Gamma^{\mu\nu\rho}, \quad (\text{A.1})$$

where,

$$\Gamma^{\mu\nu\rho}(k_1, k_2, m) = \frac{2}{i\pi^2} \int d^4 l \text{Tr} \left\{ \gamma^\rho \gamma_5 \frac{1}{\not{l} - m} \gamma^\mu \frac{1}{\not{l} + \not{k}_1 - m} \gamma^\nu \frac{1}{\not{l} + \not{k}_1 + \not{k}_2 - m} \right\}. \quad (\text{A.2})$$

The most general form of Γ consistent with QCD gauge invariance,

$$k_1^\mu \Gamma_{\mu\nu\rho} = k_2^\nu \Gamma_{\mu\nu\rho} = 0, \quad (\text{A.3})$$

can be written as,

$$\begin{aligned} \Gamma^{\mu\nu\rho} = & F_1(k_1, k_2, m) \left\{ \text{Tr}[\gamma^\rho \gamma^\nu \not{k}_1 \not{k}_2 \gamma_5] k_1^\mu + \text{Tr}[\gamma^\rho \gamma^\mu \gamma^\nu \not{k}_2 \gamma_5] k_1^\nu \right\} \\ & + F_2(k_1, k_2, m) \left\{ \text{Tr}[\gamma^\rho \gamma^\mu \not{k}_1 \not{k}_2 \gamma_5] k_2^\nu + \text{Tr}[\gamma^\rho \gamma^\mu \gamma^\nu \not{k}_1 \gamma_5] k_2^\mu \right\} \\ & + F_3(k_1, k_2, m) (k_1^\rho + k_2^\rho) \left\{ \text{Tr}[\gamma^\mu \gamma^\nu \not{k}_1 \not{k}_2 \gamma_5] \right\} \\ & + F_4(k_1, k_2, m) (k_1^\rho - k_2^\rho) \left\{ \text{Tr}[\gamma^\mu \gamma^\nu \not{k}_1 \not{k}_2 \gamma_5] \right\}. \end{aligned} \quad (\text{A.4})$$

The results for the coefficients F_i are [40, 41, 42],

$$\begin{aligned}
F_1(k_1, k_2, m) &= -I_{10} + I_{11} + I_{20}, \\
F_2(k_1, k_2, m) &= +I_{01} - I_{11} - I_{02}, \\
F_3(k_1, k_2, m) &= -I_{11}, \\
F_4(k_1, k_2, m) &= 0,
\end{aligned} \tag{A.5}$$

where,

$$I_{st} = \int_0^1 dz_1 dz_2 dz_3 \delta(1 - z_1 - z_2 - z_3) \frac{4z_1^s z_2^t}{[z_1 z_3 k_1^2 + z_2 z_3 k_2^2 + z_1 z_2 k_3^2 - m^2]}, \tag{A.6}$$

and $k_3 = (k_1 + k_2)^2$. For the particular case at hand we are interested in $k_2^2 = \varepsilon \cdot k_2 = 0$, so we get a contribution from F_1 , and in the case of off-shell W 's from F_3 . In this limit we obtain,

$$\begin{aligned}
F_1(k_1, k_2, m) &= \frac{1}{2k_1 \cdot k_2} \left[2 + 4m^2 C_0(k_1^2, 0, (k_1 + k_2)^2, m^2, m^2, m^2) \right. \\
&\quad \left. + \left(2 + \frac{k_1^2}{k_1 \cdot k_2} \right) \left[B_0((k_1 + k_2)^2, m^2, m^2) - B_0(k_1^2, m^2, m^2) \right] \right], \\
F_3(k_1, k_2, m) &= -F_1(k_1, k_2, m) \\
&\quad + \frac{1}{k_1 \cdot k_2} \left[B_0((k_1 + k_2)^2, m^2, m^2) - B_0(k_1^2, m^2, m^2) \right],
\end{aligned} \tag{A.7}$$

where,

$$\begin{aligned}
C_0(k_1^2, k_2^2, (k_1 + k_2)^2, m_1^2, m_2^2, m_3^2) &= \frac{1}{i\pi^2} \int d^d q \frac{1}{[q^2 - m_1^2][(q + k_1)^2 - m_2^2][(q + k_{12})^2 - m_3^2]}, \\
B_0(k_1^2, m_1^2, m_2^2) &= \frac{1}{i\pi^2} \int d^d q \frac{1}{[q^2 - m_1^2][(q + k_1)^2 - m_2^2]},
\end{aligned} \tag{A.8}$$

with $k_{12} = k_1 + k_2$. We now make the identification of the momenta $k_1 = p_1 + p_2, k_3 = p_3 + p_4 + p_5 + p_6, k_2 = p_7$ to calculate the physical process. To get the contribution to our process we have to multiply $T^{\mu\nu\rho}$ given in Eq. (A.1) by the tensor L , dependent on the helicity of the (12)-line and the polarization of the gluon $\varepsilon_\nu(p_7, h_7)$ with momentum p_7 . A left handed quark line adds a factor,

$$\frac{-g_s}{s_{12}} t_{i_1 i_2}^A \langle 1 - |\gamma^\mu| 2 - \rangle. \tag{A.9}$$

The decay of a Z splitting to a pair of W -bosons (which both decay to leptons) adds a factor,

$$\begin{aligned}
&\frac{-g_W^3 \cos \theta_W}{2s_{34}s_{56}(s_{127} - M_Z^2)} \left[2g^{\rho\alpha} (p_3 + p_4)^\beta - 2g^{\beta\rho} (p_5 + p_6)^\alpha + g^{\alpha\beta} (p_5 + p_6 - p_3 - p_4)^\rho \right] \\
&\times \langle 3 - |\gamma_\alpha| 4 - \rangle \langle 5 - |\gamma_\beta| 6 - \rangle \times P_W(s_{34}) P_W(s_{56}) P_Z(s_{127}).
\end{aligned} \tag{A.10}$$

Collecting terms we may define $\Lambda_{\mu\nu\rho}$ as,

$$L_{\mu\nu\rho}^A(h_1, h_7) = 8\sqrt{2}g_s g_W^3 \cos \theta_W (t^A)_{i_1 i_2} P_W(s_{34}) P_W(s_{56}) P_Z(s_{127}) \Lambda_{\mu\nu\rho}(h_1, h_7), \tag{A.11}$$

where $s_{ij} = (p_i + p_j)^2$, $s_{ijk} = (p_i + p_j + p_k)^2$ and,

$$\begin{aligned} \Lambda_{\mu\nu\rho}(h_1, h_7) &= \frac{1}{16\sqrt{2} s_{12} s_{34} s_{56} (s_{127} - M_Z^2)} \langle p_1(h_1) | \gamma_\mu | p_2(h_1) \rangle \varepsilon_\nu(p_7, h_7) \\ &\times \langle 3 - |\gamma_\alpha| 4 - \rangle \langle 5 - |\gamma_\beta| 6 - \rangle \\ &\times \left[2g^{\rho\alpha} (p_3 + p_4)^\beta - 2g^{\beta\rho} (p_5 + p_6)^\alpha + g^{\alpha\beta} (p_5 + p_6 - p_3 - p_4)^\rho \right]. \end{aligned} \quad (\text{A.12})$$

So the amplitude with a heavy doublet circulating in the loop is given by,

$$\begin{aligned} \mathcal{A}_{\text{tri}}^B(q_1^{h_1}, \bar{q}_2^{\bar{h}_1}, \nu_3, e_4^+, \mu_5^-, \bar{\nu}_6, g_7^{h_7}) &= \sum_f T_{AB}^{\mu\nu\rho}(k_1, k_2) \times L_{\mu\nu\rho} \\ &= \sum_f \frac{g_s^2}{16\pi^2} H \sqrt{2} t_{i_1 i_2}^B \{2T_3^f\} \Gamma^{\mu\nu\rho} \Lambda_{\mu\nu\rho}(h_1, h_7) \quad (\text{A.13}) \\ &= \frac{g_s^2}{16\pi^2} H \sqrt{2} t_{i_1 i_2}^B A_{\text{tri}}(q_1^{h_1}, \bar{q}_2^{\bar{h}_1}, \nu_3, e_4^+, \mu_5^-, \bar{\nu}_6, g_7^{h_7}). \end{aligned}$$

Note that with these definitions the overall factor H is the same as in Eq. (2.7) except for the extra factor of $\frac{g_s^2}{16\pi^2}$ and a sign from $2T_3^f$ depending on whether a top or bottom quark is circulating in the loop.

Defining $\mathcal{F}_i = F_i(k_1, k_2, m_t) - F_i(k_1, k_2, m_b)$ we write out in detail the case $h_1 = -1, h_7 = \pm 1$,

$$\begin{aligned} A_{\text{tri}}(q_1^L, \bar{q}_2^R, \nu_3, e_4^+, \mu_5^-, \bar{\nu}_6, g_7^R) &= \sum_f \{2T_3^f\} \Gamma^{\mu\nu\rho} \Lambda_{\mu\nu\rho}(-1, +1) \\ &= \frac{-\mathcal{F}_1[27]}{4s_{34}s_{56}(s_{127} - M_Z^2)} \left[\langle 1 - |3 + 4 - 5 - 6| 7 - \rangle \langle 35 \rangle [46] \right. \\ &\quad \left. + 2 \langle 5 - |3 + 4| 6 - \rangle \langle 13 \rangle [47] - 2 \langle 3 - |5 + 6| 4 - \rangle \langle 15 \rangle [67] \right] \\ &\quad - \frac{\mathcal{F}_3[27]^2}{4s_{12}s_{34}s_{56}(s_{127} - M_Z^2)} \langle 12 \rangle (s_{56} - s_{34}) \langle 35 \rangle [46], \end{aligned} \quad (\text{A.14})$$

$$\begin{aligned} A_{\text{tri}}(q_1^L, \bar{q}_2^R, \nu_3, e_4^+, \mu_5^-, \bar{\nu}_6, g_7^L) &= \sum_f \{2T_3^f\} \Gamma^{\mu\nu\rho} \Lambda_{\mu\nu\rho}(-1, -1) \\ &= \frac{-\mathcal{F}_1\langle 17 \rangle}{4s_{34}s_{56}(s_{127} - M_Z^2)} \left[\langle 7 - |3 + 4 - 5 - 6| 2 - \rangle \langle 35 \rangle [46] \right. \\ &\quad \left. + 2 \langle 3 - |5 + 6| 4 - \rangle \langle 75 \rangle [26] - 2 \langle 5 - |3 + 4| 6 - \rangle \langle 73 \rangle [24] \right] \\ &\quad - \frac{\mathcal{F}_3\langle 17 \rangle^2}{4s_{12}s_{34}s_{56}(s_{127} - M_Z^2)} [12] (s_{34} - s_{56}) \langle 35 \rangle [46]. \end{aligned} \quad (\text{A.15})$$

Switching between the two gluon helicities is given by $-\text{flip}_1$, with the flip_1 symmetry defined as,

$$\text{flip}_1 : 1 \leftrightarrow 2, \quad 3 \leftrightarrow 6, \quad 4 \leftrightarrow 5, \quad \langle ab \rangle \leftrightarrow [ab]. \quad (\text{A.16})$$

The cases $h_1 = +1, h_7 = \pm 1$ are simply given by,

$$A_{\text{tri}}(q_1^R, \bar{q}_2^L, \nu_3, e_4^+, \mu_5^-, \bar{\nu}_6, g_7^{L/R}) = A_{\text{tri}}(q_2^L, \bar{q}_1^R, \nu_3, e_4^+, \mu_5^-, \bar{\nu}_6, g_7^{L/R}). \quad (\text{A.17})$$

Similarly to Eq. (A.14) we define the contribution from the six massive box diagrams as,

$$\mathcal{A}_{\text{box}}^B(q_1^{h_1}, \bar{q}_2^{\bar{h}_1}, \nu_3, e_4^+, \mu_5^-, \bar{\nu}_6, g_7^{h_7}) = \frac{g_s^2}{16\pi^2} H \sqrt{2} t_{i_1 i_2}^B A_{\text{box}}(q_1^{h_1}, \bar{q}_2^{\bar{h}_1}, \nu_3, e_4^+, \mu_5^-, \bar{\nu}_6, g_7^{h_7}). \quad (\text{A.18})$$

In the next appendix we give numerical results for $A_{\text{tri}}(q_1^{h_1}, \bar{q}_2^{\bar{h}_1}, \nu_3, e_4^+, \mu_5^-, \bar{\nu}_6, g_7^{h_7})$ and $A_{\text{box}}(q_1^{h_1}, \bar{q}_2^{\bar{h}_1}, \nu_3, e_4^+, \mu_5^-, \bar{\nu}_6, g_7^{h_7})$ for a randomly chosen phase space point.

B. Explicit numerical results

In this section we present explicit numerical results for one phase space point for the independent amplitudes entering the one-loop cross sections.

We define the one-loop virtual amplitudes analogously to Eqs.(2.6, 2.8, A.14 and A.18), e.g.

$$\mathcal{A}_v^A(u_1^L, \bar{u}_2^R, \nu_3, e_4^+, \mu_5^-, \bar{\nu}_6, g_7^R) = \frac{g_s^2}{16\pi^2} \sqrt{2} t_{i_1 i_2}^A H \quad (\text{B.1})$$

$$\left[A_{7v}^{(a)}(1, 2, 3, 4, 5, 6, 7) + C_{L, \{u\}}(s_{127}) A_{7v}^{(b)}(1, 2, 3, 4, 5, 6, 7) \right],$$

and we have similar definitions for the other amplitudes.

In table 3 we present results for the colour stripped virtual amplitudes $A_{7v}^{(a)}(1, 2, 3, 4, 5, 6, 7)$ and $A_{7v}^{(b)}(1, 2, 3, 4, 5, 6, 7)$ for positive and negative quark and gluon polarizations at the following randomly chosen phase space point at the LHC – (p_x, p_y, p_z, E) [GeV] (all momenta are outgoing) at $\mu_R = 80$ GeV:

$$\begin{aligned} p_1 &= (0.00000000000000, 0.00000000000000, 1021.22119318758, -1021.22119318758), \\ p_2 &= (0.00000000000000, 0.00000000000000, -238.714576090637, -238.714576090637), \\ p_3 &= (-71.5344542606618, -183.877222508616, -3.11006048502754, 197.326337775966), \\ p_4 &= (-9.92033815503652, -76.1125676676337, 49.0057636944973, 91.0664644166627), \\ p_5 &= (32.5059044554765, 245.099246845329, -495.644737899924, 553.889863453468), \\ p_6 &= (64.1786550096635, 124.613643938661, -207.896850811885, 250.736037681104), \\ p_7 &= (-15.2297670494417, -109.723100607740, -124.860731594604, 166.917065951017). \end{aligned}$$

The poles of the one-loop unrenormalized virtual amplitudes are given by

$$A_{7v}^{a/b}(1, 2, 3, 4, 5, 6, 7) = A_7^{a/b}(1, 2, 3, 4, 5, 6, 7) \frac{\alpha_s}{4\pi} c_\Gamma \mu_R^{2\epsilon} \left(-\frac{3C_F}{\epsilon} \quad (\text{B.2}) \right.$$

$$\left. + \frac{1}{\epsilon^2} \left(N_c (-s_{17})^{-\epsilon} + N_c (-s_{17})^{-\epsilon} - \frac{1}{N_c} (-s_{12})^{-\epsilon} \right) \right). \quad (\text{B.3})$$

We renormalize the amplitude by adding the $\overline{\text{MS}}$ counterterm

$$A_{7,\text{ct}}(1, 2, 3, 4, 5, 6, 7) = -\frac{c_\Gamma}{\epsilon} b_0 \frac{\alpha_s}{8\pi} A_7(1, 2, 3, 4, 5, 6, 7), \quad (\text{B.4})$$

where

$$b_0 = \frac{11N_c - 4n_f T_R}{3}, \quad \text{and} \quad c_\Gamma = (4\pi)^\epsilon \frac{\Gamma(1+\epsilon)\Gamma^2(1-\epsilon)}{\Gamma(1-2\epsilon)}. \quad (\text{B.5})$$

Amplitude	$c_\Gamma/\epsilon^2\alpha_s/(4\pi)$	$c_\Gamma/\epsilon\alpha_s/(4\pi)$	$\alpha_s/(4\pi)$
$ A_7^a(1^R, 2^L, 3, 4, 5, 6, 7^L) $	-	-	0
$ A_{v7}^a(1^R, 2^L, 3, 4, 5, 6, 7^L) $	0	$0.413542 \cdot 10^{-16}$	$0.116250 \cdot 10^{-6}$
$ A_7^b(1^R, 2^L, 3, 4, 5, 6, 7^L) $	-	-	$0.209219 \cdot 10^{-4}$
$ A_{v7}^b(1^R, 2^L, 3, 4, 5, 6, 7^L) $	$0.118557 \cdot 10^{-3}$	$0.238602 \cdot 10^{-3}$	$0.473769 \cdot 10^{-3}$
$ A_7^a(1^L, 2^R, 3, 4, 5, 6, 7^L) $	-	-	$0.695412 \cdot 10^{-5}$
$ A_{v7}^a(1^L, 2^R, 3, 4, 5, 6, 7^L) $	$0.394067 \cdot 10^{-4}$	$0.793076 \cdot 10^{-4}$	$0.127832 \cdot 10^{-3}$
$ A_7^b(1^L, 2^R, 3, 4, 5, 6, 7^L) $	-	-	$0.686719 \cdot 10^{-5}$
$ A_{v7}^b(1^L, 2^R, 3, 4, 5, 6, 7^L) $	$0.389141 \cdot 10^{-4}$	$0.783161 \cdot 10^{-4}$	$0.125011 \cdot 10^{-3}$
$ A_7^a(1^R, 2^L, 3, 4, 5, 6, 7^R) $	-	-	0
$ A_{v7}^a(1^R, 2^L, 3, 4, 5, 6, 7^R) $	0	$0.274681 \cdot 10^{-16}$	$0.216005 \cdot 10^{-6}$
$ A_7^b(1^R, 2^L, 3, 4, 5, 6, 7^R) $	-	-	$0.171644 \cdot 10^{-4}$
$ A_{v7}^b(1^R, 2^L, 3, 4, 5, 6, 7^R) $	$0.972651 \cdot 10^{-4}$	$0.195750 \cdot 10^{-3}$	$0.352339 \cdot 10^{-3}$
$ A_7^a(1^L, 2^R, 3, 4, 5, 6, 7^R) $	-	-	$0.104711 \cdot 10^{-4}$
$ A_{v7}^a(1^L, 2^R, 3, 4, 5, 6, 7^R) $	$0.593364 \cdot 10^{-4}$	$0.119417 \cdot 10^{-3}$	$0.254739 \cdot 10^{-3}$
$ A_7^b(1^L, 2^R, 3, 4, 5, 6, 7^R) $	-	-	$0.102672 \cdot 10^{-4}$
$ A_{v7}^b(1^L, 2^R, 3, 4, 5, 6, 7^R) $	$0.581805 \cdot 10^{-4}$	$0.117091 \cdot 10^{-3}$	$0.247373 \cdot 10^{-3}$

Table 3: Numerical results for the Born and virtual amplitudes with massless particles in the loop.

Amplitude	$\alpha_s/(4\pi)$
$ A_{\text{box}}(1^R, 2^L, 3, 4, 5, 6, 7^L) $	2.9674010^{-8}
$ A_{\text{tri}}(1^R, 2^L, 3, 4, 5, 6, 7^L) $	8.4802510^{-7}
$ A_{\text{box}}(1^L, 2^R, 3, 4, 5, 6, 7^L) $	4.8394610^{-8}
$ A_{\text{tri}}(1^L, 2^R, 3, 4, 5, 6, 7^L) $	1.2007410^{-7}
$ A_{\text{box}}(1^R, 2^L, 3, 4, 5, 6, 7^R) $	7.3561010^{-8}
$ A_{\text{tri}}(1^R, 2^L, 3, 4, 5, 6, 7^R) $	1.1332510^{-6}
$ A_{\text{box}}(1^L, 2^R, 3, 4, 5, 6, 7^R) $	1.7482310^{-8}
$ A_{\text{tri}}(1^L, 2^R, 3, 4, 5, 6, 7^R) $	1.1486910^{-7}

Table 4: Numerical results for the massive triangle and box contributions to the virtual amplitude.

In table 4 we give numerical results for the finite contributions to the amplitude coming from the massive triangles and boxes.

References

- [1] ATLAS Collaboration, *Detector and Physics Performance Technical Design Report*. CERN/LHCC/99-14 (1999).
- [2] CMS Collaboration, J. Phys. G: Nucl. Part. Phys. **34** 995-1579.
- [3] S. Dawson, Nucl. Phys. B **359** (1991) 283.
- [4] A. Djouadi, M. Spira and P. M. Zerwas, Phys. Lett. B **264** (1991) 440.
- [5] R. V. Harlander, Phys. Lett. B **492** (2000) 74 [arXiv:hep-ph/0007289].
- [6] C. Anastasiou and K. Melnikov, Nucl. Phys. B **646** (2002) 220 [arXiv:hep-ph/0207004].
- [7] J. Ohnemus, Phys. Rev. D **44**, 1403 (1991).
- [8] J. M. Campbell and R. K. Ellis, Phys. Rev. D **60**, 113006 (1999) [arXiv:hep-ph/9905386].
- [9] L. J. Dixon, Z. Kunszt and A. Signer, Phys. Rev. D **60**, 114037 (1999) [arXiv:hep-ph/9907305].
- [10] S. Asai *et al.*, Eur. Phys. J. C **32S2**, 19 (2004) [arXiv:hep-ph/0402254].

- [11] T. Han, G. Valencia and S. Willenbrock, Phys. Rev. Lett. **69** (1992) 3274 [arXiv:hep-ph/9206246].
- [12] T. Figy, C. Oleari and D. Zeppenfeld, Phys. Rev. D **68** (2003) 073005 [arXiv:hep-ph/0306109].
- [13] E. L. Berger and J. Campbell, Phys. Rev. D **70** (2004) 073011 [arXiv:hep-ph/0403194].
- [14] B. Mellado, W. Quayle, Sau Lan Wu, TeV4LHC workshop, 29 April 2005; B. Mellado, W. Quayle and S. L. Wu, arXiv:0708.2507 [hep-ph].
- [15] S. Dittmaier, S. Kallweit and P. Uwer, arXiv:0710.1577 [hep-ph].
- [16] W. T. Giele and E. W. N. Glover, JHEP **0404** (2004) 029 [arXiv:hep-ph/0402152].
- [17] W. Giele, E. W. N. Glover and G. Zanderighi, Nucl. Phys. Proc. Suppl. **135** (2004) 275 [arXiv:hep-ph/0407016].
- [18] R. K. Ellis, W. T. Giele and G. Zanderighi, Phys. Rev. D **73** (2006) 014027 [arXiv:hep-ph/0508308].
- [19] C. Buttar *et al.*, *Les Houches physics at TeV colliders 2005, standard model, QCD, EW, and Higgs working group: Summary report*, arXiv:hep-ph/0604120.
- [20] V. M. Abazov *et al.* [D0 Collaboration], Phys. Rev. D **74**, 057101 (2006) [Erratum-ibid. D **74**, 059904 (2006)] [arXiv:hep-ex/0608011].
- [21] A. A. Affolder *et al.* [CDF Collaboration], Phys. Rev. D **63**, 072003 (2001).
- [22] L. J. Dixon, Z. Kunszt and A. Signer, Nucl. Phys. B **531**, 3 (1998) [arXiv:hep-ph/9803250].
- [23] U. Baur, J. A. M. Vermaseren and D. Zeppenfeld, Nucl. Phys. B **375**, 3 (1992).
- [24] Y. Kurihara, D. Perret-Gallix and Y. Shimizu, Phys. Lett. B **349**, 367 (1995) [arXiv:hep-ph/9412215].
- [25] F. Maltoni and T. Stelzer, JHEP **0302**, 027 (2003) [arXiv:hep-ph/0208156].
- [26] S. Catani and M. H. Seymour, Nucl. Phys. B **485** (1997) 291 [Erratum-ibid. B **510** (1997) 291] [arXiv:hep-ph/9605323].
- [27] G. Passarino and M. J. G. Veltman, Nucl. Phys. B **160**, 151 (1979).
- [28] R. K. Ellis, W. T. Giele and G. Zanderighi, Phys. Rev. D **72** (2005) 054018 [arXiv:hep-ph/0506196].
- [29] J. M. Campbell, R. Keith Ellis and G. Zanderighi, JHEP **0610**, 028 (2006) [arXiv:hep-ph/0608194].
- [30] R. K. Ellis, W. T. Giele and G. Zanderighi, JHEP **0605**, 027 (2006) [arXiv:hep-ph/0602185].
- [31] T. Hahn, Nucl. Phys. Proc. Suppl. **89**, 231 (2000) [arXiv:hep-ph/0005029]; T. Hahn and M. Rauch, Nucl. Phys. Proc. Suppl. **157**, 236 (2006) [arXiv:hep-ph/0601248].
- [32] A. D. Martin, W. J. Stirling and R. S. Thorne, Phys. Lett. B **636** (2006) 259 [arXiv:hep-ph/0603143].
- [33] A. D. Martin, R. G. Roberts, W. J. Stirling and R. S. Thorne, Phys. Lett. B **604** (2004) 61 [arXiv:hep-ph/0410230].
- [34] D. L. Rainwater and D. Zeppenfeld, Phys. Rev. D **60** (1999) 113004 [Erratum-ibid. D **61** (2000) 099901] [arXiv:hep-ph/9906218].

- [35] D. de Florian, M. Grazzini and Z. Kunszt, Phys. Rev. Lett. **82** (1999) 5209 [arXiv:hep-ph/9902483];
V. Ravindran, J. Smith and W. L. Van Neerven, Nucl. Phys. B **634**, 247 (2002) [arXiv:hep-ph/0201114];
C. J. Glosser and C. R. Schmidt, JHEP **0212**, 016 (2002) [arXiv:hep-ph/0209248].
- [36] S. Zhu, Phys. Lett. B **524** (2002) 283 [Erratum-ibid. B **537** (2002) 351].
- [37] J. Campbell and F. Tramontano, Nucl. Phys. B **726**, 109 (2005) [arXiv:hep-ph/0506289].
- [38] P. Nason, S. Dawson and R. K. Ellis, Nucl. Phys. B **303** (1988) 607.
- [39] B. Jager, C. Oleari and D. Zeppenfeld, JHEP **0607** (2006) 015 [arXiv:hep-ph/0603177].
- [40] S. L. Adler, Phys. Rev. **177**, 2426 (1969).
- [41] K. Hagiwara, T. Kuruma and Y. Yamada, Nucl. Phys. B **358**, 80 (1991).
- [42] K. Hagiwara, T. Kuruma and Y. Yamada, Nucl. Phys. B **369**, 171 (1992).